# Electronic and elastic properties of ε-phases Cr2-xVxN (x=0, 1, 2) from density-functional calculations

**ARTICLE** *in* JOURNAL OF ALLOYS AND COMPOUNDS · JANUARY 2014

Impact Factor: 3 · DOI: 10.1016/j.jallcom.2013.08.116



**6 AUTHORS**, INCLUDING:

Zhiqing Lv
Yan Shan University
**31** PUBLICATIONS **246** CITATIONS
SEE PROFILE

Wan-tang Fu
Yan Shan University
**55** PUBLICATIONS **374** CITATIONS
SEE PROFILE

Journal of Alloys and Compounds 583 (2014) 79–84

Contents lists available at ScienceDirect

Journal of Alloys and Compounds

journal homepage: www.elsevier.com/locate/jalcom

# Electronic and elastic properties of ε-phases $Cr_{2-x}V_xN$ ($x$ = 0, 1, 2) from density-functional calculations

Z.Q. Lv [a,b], Z.P. Shi [b], Y. Gao [a], Z.H. Wang [b], S.H. Sun [a], W.T. Fu [a,*]

[a] State Key Laboratory of Metastable Material Science and Technology, Yanshan University, Qinhuangdao 066004, China
[b] Key Laboratory of Advanced Forging & Stamping Technology and Science, Ministry of Education of China, College of Mechanical Engineering, Yanshan University, Qinhuangdao 066004, China

ARTICLE INFO

*Article history:*
Received 5 June 2013
Received in revised form 13 August 2013
Accepted 13 August 2013
Available online 28 August 2013

*Keywords:*
Phase stability
Electronic properties
Elastic properties
First principles

ABSTRACT

The electronic structures and elastic properties of ε-phases $Cr_{2-x}V_xN$ ($x$ = 0, 1, 2) are studied from first principles. The formation enthalpy of $Cr_2N$, CrVN, and $V_2N$ are −1.33, −2.30, and −3.10 eV/f.u, respectively. From the perspective of formation energy, the phase stability increases from $Cr_2N$, through VCrN, to $V_2N$. $\Delta E_f$ of VCrN is more negative than ([$Cr_2N$] + [$V_2N$])/2, which indicates that VCrN does not spontaneously change into two phases, $Cr_2N$ and $V_2N$. The ε-phases $Cr_{2-x}V_xN$ ($x$ = 0, 1, 2) are non-magnetic. The $B/G$ ratios of ε-phases $Cr_{2-x}V_xN$ ($x$ = 0, 1, 2) are higher than the critical value, which is 1.75. The Debye temperatures ($\theta_D$) of $Cr_2N$, CrVN, and $V_2N$ are 132, 134, and 136 K, respectively.



## 1. Introduction

High-nitrogen austenitic steels (HNS) possess a favorable combination of mechanical and physical properties, such as high strength, toughness, the capacity to work at cold temperatures, superb corrosion resistance, and low magnetic permeability [1,2]. Nitrogen alloying is known to improve the sliding wear resistance of austenitic steels due to an increase in the initial hardness and strain hardening. To further improve the combined properties of HNS, the addition of strong nitride formers niobium and vanadium to casting alloys has been considered, with a view to promoting desirable precipitate dispersions under controlled aging conditions [3]. However, secondary phase precipitation ($M_2N$) has significant influence on the hot workability of high alloy steels. Moreover, nitride precipitation may reduce mechanical and corrosion properties of HNS [4–7]. The Z-phase Cr(V,Nb)N precipitation is important for high Cr martensite/ferrite steel with V or Nb [8,9], whereas the ε-phase ($M_2X$) is one of the most important precipitates in high-nitrogen austenitic steels [4,5,10]. Knutsen et al. [3] studied the influence of niobium and vanadium additions on the precipitation behavior in a 24Cr–18Mn–1N austenitic stainless steel. They confirmed that niobium demonstrates a tendency to stabilize the cubic MX-type precipitates, and vanadium encourages the formation of hexagonal close-packed $M_2X$-type precipitates ε-phase $(Cr,V)_2N$. Erisir et al. [4] studied the effect of ε-phase precipitation on hot formability of high nitrogen steels. Wang et al. [5] studied the effect of hot deformation on the ε-$Cr_2N$ behavior in high nitrogen austenitic steel. Lin et al. [10] investigated the effect of the nitrogen/air ratio on ε-$Cr_2N$ formation in 24Cr–14Ni–2Mn stainless steel. Lazar et al. [11] investigated the phase stability of the Z-phase VCrN and related ternary V–Cr–N compounds, by application of the density functional theory (DFT) and an empirical temperature-dependent approach. However the structural properties and phase stability of nitride precipitations (ε-phases) after vanadium is added to HNS are not very clear.

The work presented aims to investigate phase stability and electronic properties of ε-phases $Cr_{2-x}V_xN$ ($x$ = 0, 1, 2) from first principles, and to clarify the phase stability considering energy and structure. The formation energies of ε-phases $Cr_{2-x}V_xN$ ($x$ = 0, 1, 2) are calculated and compared. We also investigate the elastic properties and Debye temperatures ($\theta_D$) of ε-phases $Cr_{2-x}V_xN$ ($x$ = 0, 1, 2).

## 2. Crystal structure and calculation details

The crystal structure of the $Cr_2N$ (ε-phases) is presented in Fig. 1. It is rhombohedral in form, with space group P-31m that includes three symmetry operations and nine atoms in the conventional cell with three formula units ($Z$ = 3) [12]. The Wyckoff positions of the atoms are: Cr 6k ($x_1$, 0, $z_1$), N 1a (0, 0, 0), and N 2d (0.333, 0.667, 0.5). When one or two layers of Cr atoms are replaced with V atoms, they form CrVN or $V_2N$ with the same structure [13] (see Fig. 1).

* Corresponding author. Tel.: +86 335 8074036; fax: +86 335 805 7068.
*E-mail addresses:* zhiqinglv@163.com (Z.Q. Lv), wtfu@ysu.edu.cn (W.T. Fu).

0925-8388/$ - see front matter © 2013 Elsevier B.V. All rights reserved.
http://dx.doi.org/10.1016/j.jallcom.2013.08.116

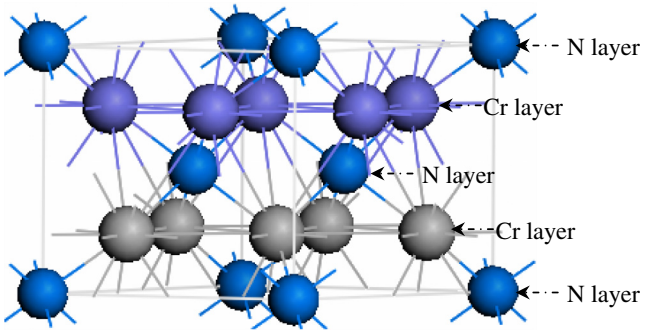


**Fig. 1.** Crystal structure of $Cr_2N$.

All calculations were performed based on the pseudo-potential plane-wave within the density functional theory [14,15], using the Cambridge Serial Total Energy Package (CASTEP) [16]. The exchange-correlation potential was evaluated using the PW91 exchange-correlation functional [17] within the generalized gradient approximation (Pw91-GGA) [18]. The interactions between the core and valence electrons were described by ultra-soft pseudo-potentials [19], and the Kohn–Sham one-electron states were expanded in a plane wave basis, set up to 400 eV. The energy calculations in the first irreducible Brillouin zone were conducted by using the $6 \times 6 \times 6$ k-point grid of the Monkhorst–Pack scheme [20]. Spin polarization was included in the calculations to correctly account for its magnetic properties. The convergence criteria for structure optimization and energy calculation were set to fine quality, with tolerance for the stress concentration factor (SCF), energy, maximum force, and maximum displacement of $10^{-6}$ eV/atom, $10^{-5}$ eV/atom, 0.03 eV/Å and 0.001 Å, respectively.

## 3. Results and discussions

### 3.1. Structural and energetic stability of the phases

The ground state properties of the ε-phases $Cr_{2-x}V_xN$ ($x = 0, 1, 2$) are investigated from their total energy, which is calculated as a function of volume. According to the Murnaghan equation of state, the equilibrium lattice constants and total energies of ε-phases $Cr_{2-x}V_xN$ ($x = 0, 1, 2$) can be obtained (see Table 1). It is found that the calculated values of the lattice constants match fairly well with the experimental values for $Cr_2N$ and $V_2N$ [12,13,21].

The energetic relative stability of $Cr_{2-x}V_xN$ ($x = 0, 1, 2$) can be discussed considering our calculations. The formation energy of a nitride $Cr_{2-x}V_xN$ ($x = 0, 1, 2$) can be defined as follows:

$$E_{\text{binding}}(Cr_{2-x}V_xN) = E_{\text{total}}(\text{unit}) - (2-x)E_{\text{isolate}}(Cr) - xE_{\text{isolate}}(V) - E_{\text{isolate}}(N) \quad (1)$$

$$\Delta E_f(Cr_{2-x}V_xN) = E_{\text{binding}}(\text{unit}) - (2-x)E_{\text{binding}}(Cr) - xE_{binding}(V) - E_{\text{binding}}(N) \quad (2)$$

**Table 1**
Experimental and calculated lattice constants $a_0$, $b_0$, $c_0$ (Å), a/c, and $v$ (Å$^3$) of ε-phases $Cr_{2-x}V_xN$ ($x = 0, 1, 2$).

| | $Cr_2N$ | | CrVN | $V_2N$ | |
|---|---|---|---|---|---|
| | Pw91 | Ref. [12] (Ref. [21]) | Pw91 | Pw91 | Ref. [13] |
| *a* | 4.7900 | 4.8004 | 4.8613 | 4.9126 | 4.9173 |
| *b* | 4.7900 | 4.8004 | 4.8613 | 4.9126 | 4.9173 |
| *c* | 4.4153 | 4.4725 | 4.4678 | 4.5512 | 4.5683 |
| *a/c* | 1.085 | 1.073 | 1.088 | 1.079 | 1.076 |
| *v* | 87.69 | 89.23 (89.585) | 91.47 | 95.12 | 95.64 |

**Table 2**
Calculated cohesive energy and formation enthalpy of ε-phases $Cr_{2-x}V_xN$ ($x = 0, 1, 2$).

| | Binding energy (eV/f.u) | Formation enthalpy (eV/f.u) | Formation enthalpy (eV/atom) |
|---|---|---|---|
| $Cr_2N$ | −33.12 | −1.33 | −0.44 |
| CrVN | −32.14 | −2.30 | −0.77 |
| $V_2N$ | −30.99 | −3.10 | −1.03 |
| $([Cr_2N]+[V_2N])/2$ | – | −2.22 | −0.74 |

Here, the binding energy and the formation enthalpy per formula unit are represented by $E_{binding}(Cr_{2-x}V_xN)$ and $\Delta E_f(Cr_{2-x}V_xN)$, respectively. $E_{total}(unit)$ is the total energy of the calculated unit, $E_{binding}(X)$ is the binding energy of pure element $X$ (X = Cr, V, N) per atom, and $E_{isolate}(X)$ denotes the total energy of an isolated $X$ atom. The binding energy of pure elements was calculated by taking their ground state conventional cell to be body centered cubic (BCC) for Cr/V and molecular $N_2$. The total energies of isolated atoms were taken from the CASTEP output files directly. It is noted that such estimations of the total energy differences (at $T = 0$ K) neglect the vibrations. At $T = 0$ K and $p = 0$ Pa, the formation enthalpy equals the calculated formation energy, *i.e.*, $\Delta H(Cr_{2-x}V_xN) = \Delta E(Cr_{2-x}V_xN)$, when the zero-vibration contribution is ignored [22,23]. The calculated cohesive energy and formation enthalpy of ε-phases $Cr_{2-x}V_xN$ ($x = 0, 1, 2$) are shown in Table 2. $\Delta E_f$ of $Cr_2N$ is −1.33 eV/f.u, $\Delta E_f$ of $V_2N$ is −3.10 eV/f.u, and $\Delta E_f$ of ε-phases CrVN is −2.30 eV/f.u. The calculated formation enthalpy of $Cr_2N$ and $V_2N$ are −1.26 and −3.03 eV/f.u, respectively, from the DFT calculations presented in the literature [11]. The $\Delta E_f$ of Z-phase VCrN with body centered tetragonal (BCT) structure ($a = 2.86$ Å, $c = 7.14$ Å), suggested by Strang and Vodarek [24], is −2.34 eV/f.u [11]. We also calculated the formation enthalpy of Z-phase ($a = 2.866$ Å, $c = 7.1618$ Å) VCrN to be −2.52 eV/f.u. The heat of formation of $Cr_2N$ was measured as 42.8 kJ mol$^{-1}$ atom$^{-1}$ (−0.44 eV/atom) at 298 K [11,25], which is in agreement with our DFT value. The formation energies of these phases are negative, which indicates that these phases are stable. From the perspective of formation energy, the phase stability increases from $Cr_2N$, through ε-phase VCrN and Z-phase VCrN, to $V_2N$. The $\Delta E_f$ of VCrN is more negative than $([Cr_2N]+[V_2N])/2$, which indicates that the VCrN (ε-phase and Z-phase) is more stable than $([Cr_2N]+[V_2N])/2$. In other words, the VCrN phase does not spontaneously change into two phases, $Cr_2N$ and $V_2N$.

### 3.2. Electronic properties

Considering the results obtained from the electronic structure of $Cr_{2-x}V_xN$ ($x = 0, 1, 2$) at equilibrium, we discuss the electronic structure from the plots of density of states (DOS). Spin polarization results from a nearly rigid band shift between the majority spins (up) to lower energy, and the minority spins (down) to higher energy, due to the energy gain from exchange. The spin-polarized total DOS and partial DOS are shown in Fig. 2, at theoretical equilibrium lattice constants. The Fermi level lies at the energy of 0 eV ($E_F = 0$ eV), and is indicated by the dash-dot line. Comparing the 'up' with 'down' DOS, the up states and down states are symmetric for these phases (see Fig. 2). The magnetic moments of these ε-phases are 0 $\mu_B$, which are calculated with up states and down states of spin-polarized DOS. This indicates the ε-phases $Cr_{2-x}V_xN$ ($x = 0, 1, 2$) are non-magnetic.

It can be seen that for $Cr_{2-x}V_xN$ ($x = 0, 1, 2$), there are five regions: (i) the lowest region is composed of Cr/V 3s states (around −72 or −64 eV); (ii) the second region is formed by Cr/V 3p states (around −43 or −38 eV); (iii) the third valence band is mainly composed of N 2s states (ranging from −17.2 to −15.4 eV); (iv) the upper valence band, which can be separated into two parts, the

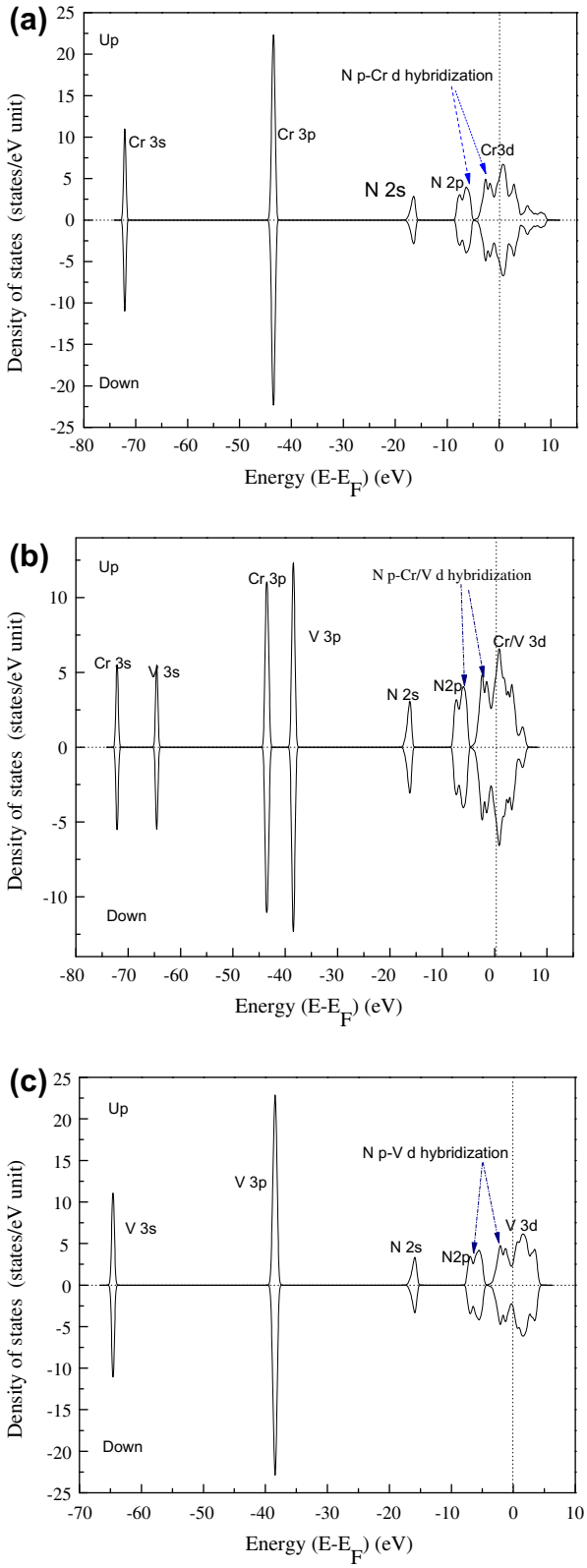


**Fig. 2.** Calculated spin-polarized DOS of (a) $Cr_2N$ (b) CrVN and (c) $V_2N$.

first from –7.6 to around –4.5 eV mainly consists of the hybridization of N 2p states and metal atom (Cr and V) 3d states; and the second, from –3.5 eV to the Fermi level, is mainly formed by metal atom (Cr and V) 3d states; and (*v*) the last energy region above $E_F$ is dominated by metal atom 4s states and unoccupied 3d states (Cr and V). There is not an energy gap observed near the Fermi level, which indicates the metallic nature of $Cr_{2-x}V_xN$ ($x$ = 0, 1, 2). Fig. 2 clearly indicates several semi-core states, like the 2s orbital of N, and the 3s and 3p orbits of Cr/V, which can be attributed to the sharp peaks in the DOS. These semi-core states have little effect on chemical bonding; but are very important in total energy calculations. Due to their largely different atomic numbers, semi-core orbits of transition metals are lower in energy than those of light elements (C and N). Generally, the resonance peak appearing in DOS can be ascribed to covalent bonds in solids. In many carbides and nitrides of transition metals, the covalence is determined by the strength of p and d hybridization. In the DOS plot of $Cr_{2-x}V_xN$ ($x$ = 0, 1, 2), the overlap between p and d orbits is obvious but not complete. This can be explained when observing the difference in the electronegativity value of the constituent elements, which leads to the ionic features of Cr/V–N bonds. In fact, transition metals form many types of carbides and nitrides, such as $Fe_3C$, VC, NbC, $Cr_7C_3$, $Fe_3N$ and $Fe_4N$, in which a mixture of bond states is always expected [26–29].

Contour plots of electron density distributions are useful for detailed analysis of the chemical bonds and charge transfer within a compound. As shown in Figs. 3 and 4, the electron density distribution map of the plane with Cr/V and N atoms is plotted in two ways; the total density map (Fig. 3), and the electron density difference map (Fig. 4). The electron density difference was determined from $\Delta\rho = \{\rho_{crystal} - \sum \rho_{at}\}$, where $\rho_{crystal}$ and $\rho_{at}$ are the valence electron densities for $Cr_{2-x}V_xN$ ($x$ = 0, 1, 2) and the corresponding free atoms, respectively. The total electron density distribution map reproduced the results obtained by Music et al. [30]. There is strong similarity in the contour plots of $Cr_{2-x}V_xN$ ($x$ = 0, 1, 2), particularly at metal atom and N atom sites, shown in Figs. 3 and 4. The densities around the Cr/V sites and N sites are almost spherical in Fig. 3. The core regions of Cr/V and N have the largest density, from Fig. 3, which is mainly due to ionic core orbits. Clearly, the density at Cr sites is much bigger than that at the V sites. That is due to the fact that there are two more 3d electrons at each Cr atom than at each V site.

Overlaps occur between the electron densities of Cr/V and N, which indicates the chemical bonding between these components. The delocalized valence electron clouds represent the metallic bonds between the metal atoms and the highest occupied energy level near the Fermi surface. Combining with DOS, we can conclude that the conduction electrons are mainly composed of the 3d electrons of a Cr/V atom. Along the bond axis, we can see a higher electron density, which is shared by both atoms in Fig. 4. The electron density difference maps reflect the exchange of electrons in space. In this paper, we selected one representative plane. On this plane, the increment of valence electrons is concentrated on the N atoms, and the elongated contours correspond to p-like orbits of N. As shown in Fig. 4, the electron densities near Cr/V atoms decrease, and the electron densities of non-metal N atoms increase. There again exists an exchange of electrons between the Cr/V atom and the N atom along the Cr/V–N direction. It is observed that the $Cr_{2-x}V_xN$ ($x$ = 0, 1, 2) bonds are a mix of metallic, covalent, and ionic.

The calculated lengths of the Cr–N bonds in the $Cr_2N$ cell are 1.9191 and 1.9465 Å, and the corresponding overlapping population values are 0.23 and 0.24, respectively. The calculated lengths of the V–N bonds in the $V_2N$ cell are 1.9957 and 1.9978 Å, and the corresponding overlapping population values are 0.20 and 0.21, respectively. The calculated lengths of the V–N bonds in the CrVN cell are 1.9937 and 1.9991 Å, and the corresponding overlapping population values are 0.16 and 0.19, respectively. Finally, the calculated lengths of the Cr–N bonds in the CrVN cell are 1.9515 and 1.9095 Å, and the corresponding overlapping population values are 0.27 and 0.28, respectively. This indicates that strong covalent bonding states exist in $Cr_{2-x}V_xN$ ($x$ = 0, 1, 2). These results agree

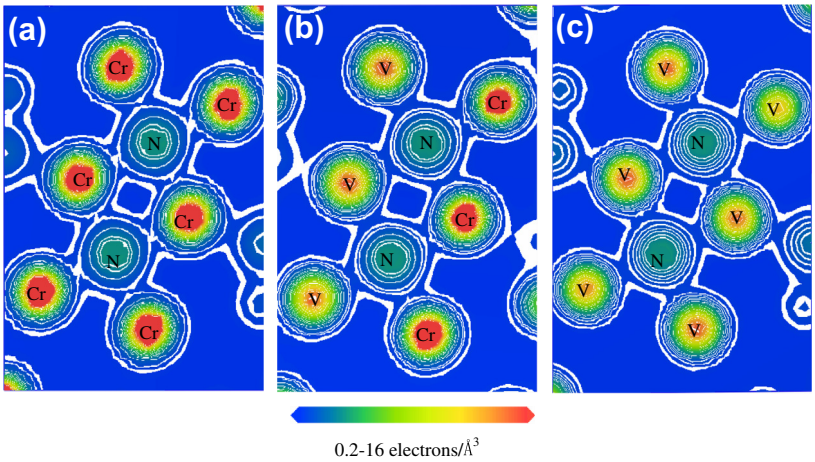


**Fig. 3.** Total electron density distribution map of the plane, with metal and N atoms plotted from 0.2 (blue) to 16 (red) eÅ$^{-3}$. Electron density values larger than 16 are neglected. (a) $Cr_2N$, (b) CrVN, and (c) $V_2N$. (For interpretation of the references to color in this figure legend, the reader is referred to the web version of this article.)

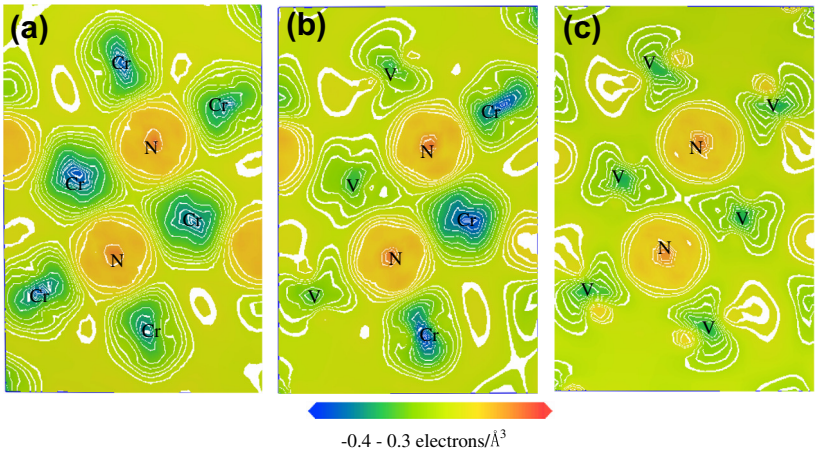


**Fig. 4.** Electron density difference map of the plane, with metal and N atoms plotted from –0.4 (blue) to 0.3 (red) eÅ$^{-3}$. (a) $Cr_2N$, (b) CrVN, and (c) $V_2N$. (For interpretation of the references to color in this figure legend, the reader is referred to the web version of this article.)

**Table 3**
Calculated elastic constants, $C_{ij}$, of $Cr_2N$, CrVN, and $V_2N$.

| Pw91 | $C_{11}$ | $C_{12}$ | $C_{13}$ | $C_{33}$ | $C_{44}$ |
|---|---|---|---|---|---|
| $Cr_2N$ | 437.7 | 135.1 | 200.0 | 381.6 | 159.7 |
| CrVN | 453.6 | 162.1 | 205.4 | 395.2 | 163.7 |
| $V_2N$ | 438.1 | 152.7 | 178.8 | 432.0 | 158.6 |

with the above electron densities map and DOS analyses of $Cr_{2-x}V_xN$ ($x$ = 0, 1, 2).

### 3.3. Elastic properties of the phases

The mechanical stability of a crystal implies that the strain energies are positive. The mechanical stability of the crystal is described with elastic constants $C_{ij}$, depending on the crystal structure. For the hexagonal crystal structures, there are five different symmetry elements, $C_{11}$, $C_{33}$, $C_{44}$, $C_{12}$, and $C_{13}$. The stability criteria for a hexagonal crystal are [22,31]:

$$C_{11} > 0, C_{11} - C_{12} > 0, C_{44} > 0, (C_{11} + C_{12})^* C_{33} - 2C_{13}^2 > 0 \quad (3)$$

As shown in, Table 3. the elastic constants $C_{ij}$ of ε-phases $Cr_2N$, CrVN, and $V_2N$ were calculated using their equilibrium lattice constants and optimized structure. From the results, we find ε-phases $Cr_{2-x}V_xN$ ($x$ = 0, 1, 2) are mechanically stable as their elastic constants satisfy inequalities (3).

A problem arises when single crystal samples cannot be obtained. It is then impossible to measure the individual elastic constants $C_{ij}$. Instead, the isotropic bulk modulus, $B$, and shear modulus, $G$, are determined [32]. These quantities cannot in general be calculated directly from $C_{ij}$, but we can use our values to place bounds on the isotropic moduli. Reuss [33] found lower bounds for all lattices, while Voigt [34] discovered upper bounds. Hill [35] showed that the Voigt and Reuss averages were limits, and suggested that the actual effective moduli could be approximated by the arithmetic mean of the two bounds. The formulas for these bounds for hexagonal lattices can be found in the literature [32]. We also calculated Young's modulus ($E$) and Poisson's ratio ($v$). These quantities relate to the bulk modulus and the shear modulus by the following equations [36]:

$$E = 9BG/(3B + G) \quad (4)$$

$$v = (3B - E)/6B \quad (5)$$

The calculated Voigt's bulk modulus ($B_v$), Reuss's bulk modulus ($B_R$), effective bulk modulus ($B$), Voigt's shear modulus ($G_v$), Reuss's shear modulus ($G_R$), effective shear modulus ($G$), Young's modulus ($E$), and Poisson's ratio ($v$) of ε-phases $Cr_{2-x}V_xN$ ($x$ = 0, 1, 2) are given in

**Table 4**
Calculated Voigt's bulk modulus ($B_v$), Reuss's bulk modulus ($B_R$), effective bulk modulus ($B$), Voigt's shear modulus ($G_v$), Reuss's shear modulus ($G_R$), effective shear modulus ($G$), Young's modulus ($E$, in GPa), and Poisson's ratio ($v$) for $Cr_2N$, CrVN, and $V_2N$.

| | $B_V$ | $B_R$ | $B$ | $G_V$ | $G_R$ | $G$ | $B/G$ | $E$ | $v$ |
|---|---|---|---|---|---|---|---|---|---|
| $Cr_2N$ | 258.7 | 258.7 | 258.7 | 142.2 | 134.8 | 138.5 | 1.88 | 353.0 | 0.273 |
| CrVN | 272.0 | 271.9 | 271.9 | 143.3 | 137.9 | 140.6 | 1.93 | 359.8 | 0.279 |
| $V_2N$ | 258.7 | 258.6 | 258.7 | 145.2 | 141.0 | 143.1 | 1.81 | 362.5 | 0.266 |

Table 4. The calculated bulk modulus value of $Cr_2N$ agrees with the measured value, 275(23) GPa [21].

The ratio of $B$ to $G$ gives us an estimation of the degree of ductility [37]. The ratios of ε-phases $Cr_{2-x}V_xN$ ($x$ = 0, 1, 2) are higher than the critical value 1.75, separating ductile and brittle behavior of a material [37]. The bigger the ratio, the higher the ductility is. It can be seen that the three phases are not brittle materials. The bulk modulus of ε-phases CrVN is the biggest of the three phases, and the ductility of ε-CrVN (1.93) is better than that of $Cr_2N$ and $V_2N$.

### 3.4. Calculation of Debye temperature

Debye temperature is a fundamental parameter closely related to many physical properties, such as elastic constants, specific heat, and melting point. One of the standard methods used to calculate the Debye temperature ($\theta_D$) is to use the elastic constant data, since $\theta_D$ may be estimated from the average sound velocity, $v_m$, by the following equation [38]:

$$\theta_D = \frac{h}{k_B}\left[\frac{3n}{4\pi V}\right]^{1/3} v_m \quad (6)$$

where $h$ is Planck's constant, $k_B$ is Boltzmann's constant, $n$ is the number of atoms in the unit cell, and $V$ is the cell volume. The average sound velocity in the polycrystalline material is given by [36]:

$$v_m = \left[\frac{1}{3}\left(\frac{2}{v_t^3}+\frac{1}{v_l^3}\right)\right]^{-1/3} \quad (7)$$

where $v_l$ and $v_t$ are the longitudinal and transverse sound velocity obtained using the shear modulus $G$ and the bulk modulus $B$ from Navier's equation [36]:

$$v_t = \left(\frac{3B+4G}{3\rho}\right)^{\frac{1}{2}} \quad (8)$$

$$v_l = \left(\frac{G}{\rho}\right)^{\frac{1}{2}} \quad (9)$$

Heat capacity is an invaluable tool when exploring the fundamental properties of materials, as it probes low-lying excitations, and the experimental results can be directly compared with calculations from first principles. For metallic-like, three-dimensional materials at the lowest temperatures, the constant pressure heat capacity, $C_p$, can be approximated by the well-known relationship [39]:

$$C_p = \gamma T + \beta T^3 \quad (10)$$

where $\gamma$ is related to the electron density of states, and $\beta$ relates to the phonon excitations. N($E_F$) is the electron state at the Fermi level. The $\gamma$ term is given by [40]:

$$\gamma = \frac{\pi^2 k_B^2 N(E_F)}{3}. \quad (11)$$

When considering the phonon contribution to $C_p$, the parameter typically reported is the Debye temperature, $\theta_D$, which is related to $\beta$ by [40]:

**Table 5**
Calculated longitudinal, transverse and average sound velocity ($v_l$, $v_t$, $v_m$, in m/s) from the polycrystalline elastic modulus, the Debye temperature ($\theta_D$, in K), the average electronic heat capacity contribution ($\gamma$, in $10^{-2}$ J/mol K$^2$), and the average phonon heat capacity contribution ($\beta$, in $10^{-4}$ J/mol K$^4$), for $Cr_2N$, CrVN, and $V_2N$.

| | $v_l$ | $v_t$ | $v_m$ | $\theta_D$ | $\gamma$ | $\beta$ |
|---|---|---|---|---|---|---|
| $Cr_2N$ | 4548.7 | 8135.0 | 5936.4 | 132 | 1.16 | 8.49 |
| CrVN | 4698.1 | 8492.0 | 6148.1 | 134 | 0.99 | 7.97 |
| $V_2N$ | 4855.4 | 8605.4 | 6321.7 | 136 | 0.66 | 7.62 |

$$\theta_D^3 = \frac{4\pi^4 R}{5\beta} N \quad (12)$$

where $N$ is the number of models (atoms) per formula unit, and $R$ is the molar gas constant. The calculated sound velocity, Debye temperature, $\gamma$, and $\beta$ of $Cr_{2-x}V_xN$ ($x$ = 0, 1, 2) are given in Table 5. The Debye temperatures ($\theta_D$) of $Cr_2N$, CrVN, and $V_2N$ are 132 K, 134 K and 136 K, respectively. This indicates that the thermo-stabilities of $Cr_{2-x}V_xN$ ($x$ = 0, 1, 2) are similar.

## 4. Conclusion

In summary, a complete theoretical analysis of the electronic and elastic properties of ε-phases $Cr_{2-x}V_xN$ ($x$ = 0, 1, 2) has been presented, by means of calculation from first principles. The calculated equilibrium structural parameters of $Cr_2N$ and $V_2N$ are in agreement with the experimental results. Using the same calculation method, the crystal structure of ε-CrVN is predicted. $\Delta E_f$ of $Cr_2N$ is −1.33 eV/f.u, $\Delta E_f$ of $V_2N$ is −3.10 eV/f.u, and the $\Delta E_f$ of ε-phases CrVN is −2.30 eV/f.u. We also calculated the formation enthalpy of Z-phase VCrN as −2.52 eV/f.u. The formation energy value of $Cr_2N$ in our DFT is in agreement with the measured value. The formation energies of these phases are negative, which indicates that these phases are stable. From the perspective of formation energy, the phase stability increases from $Cr_2N$, through ε-phase VCrN and Z-phase VCrN, to $V_2N$. $\Delta E_f$ of VCrN is more negative than ([$Cr_2N$]+[$V_2N$])/2, which indicates that VCrN (ε-phase and Z-phase) is more stable than ([$Cr_2N$]+[$V_2N$])/2. In other words, the VCrN phase does not spontaneously change into two phases, $Cr_2N$ and $V_2N$. Comparing the 'up' with 'down' density of states, the up states and down states are symmetric for these phases; this indicates that the ε-phases $Cr_{2-x}V_xN$ ($x$ = 0,1,2) are non-magnetic. From analysis of the electron density of $Cr_{2-x}V_xN$ ($x$ = 0, 1, 2), it is confirmed that the bonds of ε-phases $Cr_{2-x}V_xN$ ($x$ = 0, 1, 2) are a complex mixture of metallic, covalent and ionic bonds. The bulk modulus ($B$), shear modulus ($G$), Young's modulus ($E$), and Poisson's ratio ($v$) of ε-phases $Cr_{2-x}V_xN$ ($x$ = 0, 1, 2) were calculated. The $B/G$ ratios of ε-phases $Cr_{2-x}V_xN$ ($x$ = 0, 1, 2) are higher than the critical value (1.75). The Debye temperatures ($\theta_D$) of $Cr_2N$, CrVN, and $V_2N$ are 132 K, 134 K and 136 K, respectively.

## Acknowledgements

This research was supported by the Natural Science Foundation of China (Nos. 51101137 and 51171161).

## References

[1] V.G. Gavriljuk, H. Berns, High Nitrogen Steels, Springer-Verlag, Berlin, 1999.
[2] Uggowitzer PJ, Madowski R, Speidel MO. In: Proceedings of the Innovative Stainless Steels, Florence, Italy, 1993. p. 2. 359.
[3] R.D. Knutsen, C.I. Lang, J.A. Basson, Acta Mater. 52 (2004) 2407–2417.
[4] E. Erisir, U. Prahl, W. Bleck, Mater. Sci. Eng.A 528 (2010) 519–525.
[5] Z.H. Wang, W.T. Fu, S.H. Sun, et al., J. Mater. Eng. Perform. 19 (2010) 951–954.
[6] J.A. Cotton, R.D. Knutsen, C.I. Lang, Mater. Sci. Forum. 271 (1999) 318–320.
[7] J.W. Simmons, Scr. Metall. Mater. 32 (1995) 265–270.
[8] C. Kocer, T. Abe, A. Soon, Mater. Sci. Eng. A 505 (2009) 1–5.

[9] L. Cipolla, H.K. Danielsen, P.E. Di Nunzio, D. Venditti, J. Hald, M.A.J. Somers, Scr. Mater. 63 (2010) 324–327.
[10] D.Y. Lin, G.L. Liu, T.C. Chang, H.C. Hsieh, J. Alloys Comp. 377 (2004) 150–154.
[11] P. Lazar, R. Podloucky, E. Kozegnscik, J. Redinger, Phys. Rev. B 78 (2008) 134202.
[12] T.H. Lee, S.J. Kim, E. Shin, S. Takaki, Acta Crystallogra. B 62 (6) (2006) 979–986.
[13] A.N. Christensen, B. Lebech, Acta Crystallogra. B 35 (11) (1979) 2677–2678.
[14] W. Kohn, L.J. Sham, Phys. Rev. A 140 (1965) 1133.
[15] P. Hohenberg, W. Kohn, Phys. Rev. B 136 (1964) 384.
[16] M.D. Segall, P.J.D. Lindan, M.J. Probert, C.J. Pichard, P.J. Hasnip, S.J. Clark, M.C. Payne, J. Phys. Condens. Mater. 14 (2002) 2717.
[17] J.P. Perdew, J.A. Chevary, S.H. Vosko, K.A. Jackson, M.R. Pederson, D.J. Singh, C. Fiolhais, Phys. Rev. B 46 (1992) 6671–6687.
[18] J.P. Perdew, K. Burke, M. Ernzerhof, Phy. Rev. Lett. 77 (1996) 3865.
[19] D. Vanderbilt, Phys. Rev. B 41 (1990) 7892.
[20] H. Jmonkhorst, J.D. Pack, Phys. Rev. B 13 (1976) 5188.
[21] E. Soignard, O. Shebanova, P.F. McMillan, Phys. Rev. B 75 (2007) 014104.
[22] W.H. Zhang, Z.Q. Lv, Z.P. Shi, S.H. Sun, Z.H. Wang, W.T. Fu, J. Magn. Magn. Mater. 324 (2012) 2271–2276.
[23] C.M. Fang, M.H.F. Sluiter, M.A. Van Huis, C.K. Ande, H.W. Zandbergen, Phys. Rev. Lett. 105 (2010) 055503.
[24] A. Strang, V. Vodarek, Mater. Sci. Technol. 12 (1996) 552.
[25] A.D. Mah, US Bureau Mines, Representative Investment Technical, Report No. 5529, 1969.
[26] J.R. Kitchin, J.K. Norskov, M.A. Barteau, Physica B 371 (2006) 126.
[27] Z.Q. Lv, W.T. Fu, S.H. Sun, Z.H. Wang, W. Fan, M.G. Qv, Solid State Sci. 12 (2010) 404.
[28] Z.Q. Lv, S.H. Sun, Y. Gao, Z.H. Wang, Z.P. Shi, W.T. Fu, J. Magn. Magn. Mater. 333 (2013) 39–45.
[29] B. Xiao, J.D. Xing, J. Feng, Y.F. Li, C.T. Zhou, W. Su, Physica B 403 (2008) 2273–2281.
[30] D. Music, U. Kreissig, R. Metens, J.M. Schneider, Phys. Lett. A 326 (2004) 473.
[31] Z.J. Wu, E.J. Zhao, H.P. Xiang, X.F. Hao, X.J. Liu, J. Meng, Phys. Rev. B 76 (2007) 054115.
[32] M.J. Mehl, B.M. Barry, D.A. Papaconstantopoulos, Intermetallic compounds: principle and practice, in: J.H. Westbrook, R.L. Fleischeir (Eds.), vol. 1: Principles, Wiley, London, 1995, p. 195.
[33] A. Reuss, Z. Angew, Math. Mech. 8 (1929) 55.
[34] W. Voigt, Lehrbush der Kristallphysik, Taubner, Leipzig, 1928.
[35] R. Hill, Proc. Phys. Soc. London A 65 (1952) 349.
[36] E. Schreiber, O.L. Anderson, N. Soga, Elastic Constants and their Measurements, McGraw-Hill, New York, 1973.
[37] S.Q. Wu, Z.F. Hou, Z.Z. Zhu, Solid State Sci. 11 (2008) 251.
[38] V. Kanchana, G. Vaitheeswaran, A. Savane, A. Delin, J. Phys, Condens. Matter. 18 (2006) 9615.
[39] M.K. Drulis, H. Drulis, S. Gupta, M.W. Barsoum, T. El-Raghy, J. Appl. Phys. 99 (2006) 093502.
[40] M.K. Drulis, H. Drulis, A.E. Hachemer, A. Ganguly, T. El-Raghy, M.W. Barsoum, J. Alloys Comp. 433 (2007) 59.